

RESEARCH

Open Access



N'-(Furan-2-ylmethylene)-2-hydroxybenzo-hydrazide and its metal complexes: synthesis, spectroscopic investigations, DFT calculations and cytotoxicity profiling

Nasser M. Hosny^{1*}, Ghada Samir¹ and Mohamed H. Abdel-Rhman^{2*}

Abstract

The ligand, *N'*-(furan-2-ylmethylene)-2-hydroxybenzohydrazide (H_2L), was synthesized characterized through various spectral studies which cleared out that the free ligand existed in keto form. The ligand upon reaction with Cu(II), Co(II), Ni(II) and Zn(II) acetates yielded complexes with stoichiometric ratio 1:2 (M:L) which has been validated through the elemental and mass spectral measurements. The IR and NMR spectral studies of the isolated complexes disclosed that the ligand chelated to metal ion in mononegative bidentate fashion via the azomethine nitrogen and deprotonated enolized carbonyl oxygen. Moreover, the DFT quantum chemical calculations designated that the ligand and Ni(II) complex exhibited the highest and lowest values of HOMO, LUMO energies and HOMO-LUMO energy gap, respectively. Furthermore, the in vitro cytotoxic activity towards HePG-2 and HCT-116 cell lines of the isolated compounds was investigated and the data cleared out that the ligand was more potent than the metal complexes.

Keywords Schiff's base, Metal complexes, DFT computation, Spectral studies, Cytotoxicity

Introduction

Since their first discovery by Hugo Schiff in 1864, the Schiff bases have been received significant attention owing to their facile synthesis by condensation reaction of primary amines with carbonyl compounds, such as aldehydes or ketones [1]. In coordination chemistry, Schiff base have been considered as a unique class of ligands due to their incorporate diverse donor groups

and exhibiting good flexibility [2, 3]. Consequently, their metal complexes are significant because of its stability, capability to form metal chelates in mono-, bi- and polydentate manner, and wide range biological applications [4–9]. Additionally, several Schiff bases were exhibited potent antibacterial, antifungal, anticancer and diuretic activities and were widely utilized in food and dye industry, analytical chemistry, catalysis and agro-chemical activities [10]. The biological activities of these compounds may be attributed to the presence of azomethine nitrogen, C=N, which serves as binding site for metal ions to interact with various biomolecules like proteins and amino acids [11].

Among the Schiff bases, heterocyclic derivatives possessed nitrogen and oxygen atoms as electron donors

*Correspondence:

Nasser M. Hosny
Nasser_Hosny@sci.psu.edu.eg; Nasserh56@yahoo.com

Mohamed H. Abdel-Rhman
mhassan2371@yahoo.com

Full list of author information is available at the end of the article



© The Author(s) 2024. **Open Access** This article is licensed under a Creative Commons Attribution 4.0 International License, which permits use, sharing, adaptation, distribution and reproduction in any medium or format, as long as you give appropriate credit to the original author(s) and the source, provide a link to the Creative Commons licence, and indicate if changes were made. The images or other third party material in this article are included in the article's Creative Commons licence, unless indicated otherwise in a credit line to the material. If material is not included in the article's Creative Commons licence and your intended use is not permitted by statutory regulation or exceeds the permitted use, you will need to obtain permission directly from the copyright holder. To view a copy of this licence, visit <http://creativecommons.org/licenses/by/4.0/>. The Creative Commons Public Domain Dedication waiver (<http://creativecommons.org/publicdomain/zero/1.0/>) applies to the data made available in this article, unless otherwise stated in a credit line to the data.

were heavily studied because of their therapeutic potentials against certain types of tumors [12, 13]. For example, the furan Schiff base derivatives and its metal complexes behaved as bidentate ligands via azomethine-N and furanyl-O which were the sites potentially responsible for the enhancement of biological activity [14]. Correspondingly, the furan-based Schiff base derivatives exhibit substantial antituberculosis, anti-inflammatory, antibacterial, anti-fungal and anticancer activities [15–18].

As well, the benzohydrazide derivatives and its metal complexes have been employed in many biological applications, as anti-inflammatory, antibacterial, and anticancer agents. The significant biological activity and extensive range of uses of benzohydrazide may be attributed to the presence of its potential keto-enol tautomeric forms, which arise from the electron delocalization between the adjacent amine and carbonyl groups [8, 19–22].

In contrast, the Cu(II), Co(II), Ni(II), and Zn(II) complexes were examined for their adjustable electrical and spectroscopic characteristics, as well as their diverse structural functionality, which is essential for targeted applications. Moreover, they play a crucial role as an essential component in several enzymes, including urease and hydrogenases [23]. Furthermore, the metal-based medications were effectively capable to pass through the microbial membrane and exhibit strong binding affinities towards the genetic materials (RNA or DNA) of these pathogenic microorganisms [12, 13, 24].

Therefore, in continuation of our former endeavors to developing hydrazide-based hybrids and their transition metal complexes that may have anticancer activity [25–31], the present study presents the synthesis, characterization and anticancer application of the newly synthesized ligand, *N'*-(furan-2-ylmethylene)-2-hydroxybenzohydrazide, and its Cu(II), Co(II), Ni(II) and Zn(II) complexes.

Experimental

Materials and instruments

Furan-2-carbaldehyde (99%), 2-hydroxybenzohydrazide (99%) and metal acetate salts were of analytical grade (A.R. from Sigma-Aldrich or Merck). Fetal Bovine serum was purchased from GIBCO, UK, while the cell lines, hepatocellular (HePG-2) and colon (HCT-116) carcinoma were obtained from ATCC, Egypt. Both tetrazolium bromide (MTT) and RPMI-1640 medium were brought from Sigma Co., USA.

The carbon, hydrogen and nitrogen contents were determined on CHN analyzer Perkin-Elmer model 2400. The metals content were determined by standard methods [32]. The Thermo-Nicolet IS10 spectrometer employed for recording the FT-IR spectra, as KBr discs.

The Unicam UV/Vis UV2 spectrometer used to measure the electronic spectra in 1 cm silica cells. The ¹H NMR spectra were recorded on Bruker Ascend spectrometer 400 MHz. The Electron spin resonance spectra were recorded at room temperature on Brucker E 500 ESR spectrometer operating at 9.808 GHz, 100 kHz field modulation from 480 to 6480 Gauss in a 2 mm quartz capillary. TGA was measured on a Schimadzu model 50 instrument using heating rate 15 °C/min at 10 cm³/min nitrogen flow rate. The mass spectra were recorded on Varian MAT 311 spectrometer. Magnetic measurements were carried out on a Sherwood Scientific magnetic balance.

Mass spectra were made on instrument.

Synthesis of the ligand (H_2L) and metal complexes

Furan-2-carbaldehyde (1.2 mL, 0.01 mol) was added drop wise to ethanolic solution of 2-hydroxybenzohydrazide (1.52 g, 0.01 mol) then a few drops of glacial acetic acid were added. The reaction mixture was heated under reflux for 4 h where a faint brown precipitate of *N'*-(furan-2-ylmethylene)-2-hydroxybenzohydrazide was formed [33]. While hot, the precipitate was filtered off, washed successfully with ethanol, dried and recrystallized from hot ethanol (m.p.: 190 °C).

To ethanolic solution of H_2L (0.02 mol), a water solution of the Cu(II), Co(II), Ni(II) or Zn(II) acetate (0.01 mmol) were added dropwise with stirring. The reaction mixture was refluxed for 2 h [22, 33]. The precipitates were filtered off, washed with hot ethanol followed by diethyl ether and dried in a vacuum desiccator over anhydrous $CaCl_2$.

DFT computations

The computational study of the isolated ligand (H_2L) and its bivalent metal complexes was carried out using Gaussian 09 W [34] to explore their geometries. The geometrical optimization was proceeded for the neutral ground state in gas phase without any symmetry constraints [12, 13] at B3LYP level and 6-31++G(d,p) basis set [35–37]. The HOMO-LUMO illustrations were made by GaussView program [38].

Cytotoxicity assay

The ligand and its metal complexes cytotoxic activity examination was performed by the MTT assay using doxorubicin as a standard anticancer drug for comparison. The cell lines were cultured in RPMI-1640 medium (10% fetal bovine serum). Antibiotics (100 units/mL penicillin and 100 µg/mL streptomycin) were added in a 5% CO₂ at 37 °C incubator. The cells were incubated with the tested compounds for 24 h. After incubation time, 20 µL of tetrazolium bromide (MTT) solution (5 mg/mL)

was incubated for four hours. Dimethyl sulfoxide (100 μL) was added to the formed purple formazan, then, the absorbance was measured at 570 nm using a plate reader (EXL 800, USA). The percentage of relative cell viability was calculated as $(A_{570} \text{ of treated samples}/A_{570} \text{ of untreated sample}) \times 100$ [39, 40].

Results and discussion

The ligand, N' -(furan-2-ylmethylene)-2-hydroxybenzohydrazide (H_2L), elemental analyses (Table 1) revealed that it has $\text{C}_{12}\text{H}_{10}\text{N}_2\text{O}_3$ formula while its metal complexes had a 1:2 (M:L) stoichiometric, i.e., bis(N -(furan-2-ylmethylene)-2-hydroxybenzohydrazonate) cobalt(II), nickel(II), copper(II) and zinc(II) monohydrate. The metal complexes were soluble in DMF and DMSO only and exhibited molar conductivity, in DMSO, $3.2\text{--}8.1 \Omega^{-1} \text{ cm}^2 \text{ mol}^{-1}$ which indicated their non-electrolytic nature [41].

FT-IR spectra

The ligand (H_2L) has two possible tautomeric forms, keto and enol, as shown in Structure 1, therefore, its IR spectrum was carefully studied in order to determine in which form the ligand is existed. The spectrum displayed sharp band at 3248 cm^{-1} with a shoulder at 3142 cm^{-1} ascribed to the hydroxyl group $\nu(\text{OH})$ [33, 42, 43] and hydrazone NH [33, 43], respectively. In addition, the strong band at 1635 cm^{-1} with shoulder at 1610 cm^{-1} were designated to the carbonyl $\nu(\text{C=O})$ [33, 43] and azomethine $\nu(\text{C=N})$ [33, 43], respectively. Furthermore, the aromatic $\nu(\text{C=C})$ along with the furane $\nu_{\text{as}}(\text{C-O-C})$ and $\nu_s(\text{C-O-C})$ vibrations [44, 45] were observed at 1588 , 1237 and 1017 cm^{-1} , respectively (Fig. 1). Hence, the abovementioned findings implied that the carbonyl and hydrazone NH were present which advocated the keto-form of the free ligand. Also, the sharpness of the vibrational band $\nu(\text{OH})$ along with the lower shift of $\nu(\text{C=O})$ suggested their involvement in H-bond formation [42] (Table 2).

The spectra of metal complexes showed one broad band at $3436\text{--}3452 \text{ cm}^{-1}$ which was attributed to the

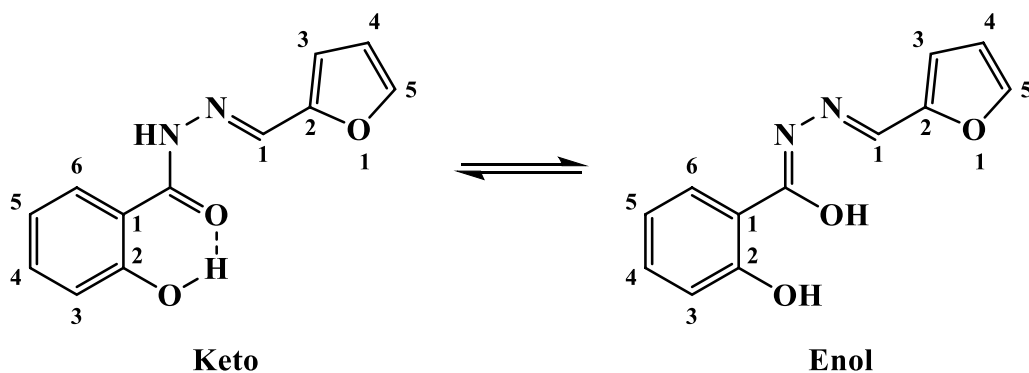
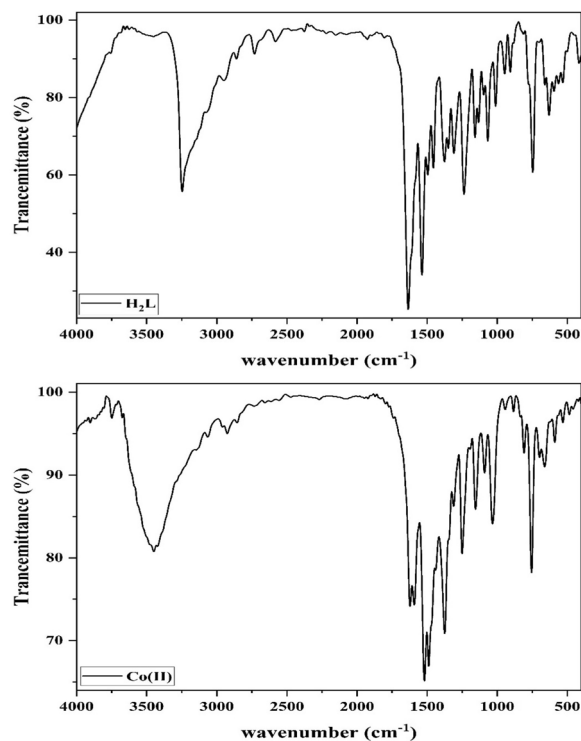
hydroxyl $\nu(\text{OH})$ vibration where the position shift and broadness, with respect to that of the ligand, suggested that the hydroxyl group was free (no H-bond). Moreover, the two bands at $1620\text{--}1628$ and $1589\text{--}1599 \text{ cm}^{-1}$ regions were assigned to the azomethine $\nu(\text{C=N})$ [33, 43] and aromatic $\nu(\text{C=C})$ [33, 43], respectively (Fig. 1). Furthermore, the furane $\nu_{\text{as}}(\text{C-O-C})$ and $\nu_s(\text{C-O-C})$ vibrations [44, 45] were observed at about 1242 and 1020 cm^{-1} , respectively, in all complexes except in Co(II) complex, where both were displayed at higher wavenumbers, 1257 and 1035 cm^{-1} . Thus, the disappearance of both the carbonyl $\nu(\text{C=O})$ and hydrazone NH with appearance of the $\nu(\text{C=N})$ vibration band disclosed that the ligand existed in enol form. But, the absence of new band due to the newly formed OH group supported the deprotonation of such group on reaction with metal salt. The Amide II and $\nu(\text{C=N})$ bands shift to lower position indorsed the ligand enolization and involvement of the azomethine groups in coordination to the metal ion. The higher shift of the furan bands in Co(II) complex was taken as evidence for participation of the furan oxygen in chelating the metal ion. Furthermore, the new bands at $565\text{--}592$ and $445\text{--}488 \text{ cm}^{-1}$ regions were attributed to $\nu(\text{M-O})$ and $\nu(\text{M-N})$ [46–48], respectively (Additional file 1: Fig. S1). The above-mentioned foundations suggested that the ligand chelated to the metal ion in enol form as mononegative bidentate or tridentate via C=N , the deprotonated enolic hydroxyl group or furan oxygen (Scheme 1).

NMR spectra

The ligand $^1\text{H-NMR}$ spectrum, in DMSO-d_6 , showed two multiplet signals at 6.65 and 6.97 ppm assigned to the protons of the furan at 3,4-positions and phenyl at 3,5-positions [42, 49], respectively. The triplet signal at 7.44 ppm was corresponded to phenyl at 4-position whereas the doublet signal present at 7.86 was attributed to the overlapping of phenyl-6 and furan-5 [42, 49].

Table 1 Elemental analyses of H_2L and the isolated metal complexes

Compound (formula; M.Wt. g/mol)	Color	M.P. (°C)	Elemental analysis % Found (calculated)			
			C	H	N	M
H_2L ($\text{C}_{12}\text{H}_{10}\text{N}_2\text{O}_3$; 232.22)	Beige	190	62.86 (62.61)	4.48 (4.38)	12.61 (12.17)	–
$[\text{Co}(\text{HL})_2]$ ($\text{C}_{24}\text{H}_{18}\text{CoN}_4\text{O}_6$; 517.36)	Brown	> 300	55.41 (55.72)	3.83 (3.51)	11.06 (10.83)	11.55 (11.39)
$[\text{Ni}(\text{HL})_2]$ ($\text{C}_{24}\text{H}_{18}\text{NiN}_4\text{O}_6$; 517.12)	Orange	> 300	55.48 (55.74)	3.72 (3.51)	11.18 (10.83)	10.90 (11.35)
$[\text{Cu}(\text{HL})_2]$ ($\text{C}_{24}\text{H}_{18}\text{CuN}_4\text{O}_6$; 521.98)	Pale green	> 300	55.63 (55.23)	3.28 (3.48)	11.35 (10.73)	11.82 (12.17)
$[\text{Zn}(\text{HL})_2](\text{H}_2\text{O})$ ($\text{C}_{24}\text{H}_{20}\text{ZnN}_4\text{O}_7$; 541.83)	Yellow	> 300	53.19 (53.20)	3.75 (3.72)	9.93 (10.34)	11.80 (12.07)

**Structure 1** The possible tautomeric forms of the ligand**Fig. 1** IR spectra of H_2L and Co(II) complex

Moreover, the two singlet signal at 8.37 and 11.80 ppm were ascribed to azomethine proton ($\text{HC}=\text{N}$) and both of phenolic OH and hydrazonyl NH [42, 49], respectively. The appearance of the phenolic OH overlapped with the NH proton confirms that the ligand exists in the keto form and involvement of OH in H-bond [29, 30] (Fig. 2A). On the other hand, the spectrum of Zn(II) complex, in $\text{DMSO}-\text{d}_6$, showed a singlet signal at 13.98 ppm that was designated to the free phenolic proton (OH) [29, 30]. The other singlet signal at 8.59 ppm was ascribed to the azomethine proton ($\text{HC}=\text{N}$) [42, 50]. The appearance of only one signal due to the phenolic OH proton

Table 2 Some IR bands of H_2L and the isolated metal complexes

Bands	H_2L	Cu(II)	Co(II)	Ni(II)	Zn(II)
$\nu(\text{OH})_{\text{solv}}$	3248*	3449	3452	3448	3436
$\nu(\text{NH})$	3142	–	–	–	–
$\nu(\text{CH})_{\text{Ar}}$	3072	3066	3062	3084	3063
$\nu(\text{C}=\text{O})$	1635	–	–	–	–
$\nu(\text{C}=\text{N})$	1610*	1620	1622	1628	1625
$\nu(\text{C}=\text{C})$	1588	1599	1592	1592	1589
Amide II	1537	1517	1519	1521	1520
$\nu_{\text{as}}(\text{C}-\text{O}-\text{C})_{\text{furan}}$	1237	1241	1257	1243	1242
$\nu(\text{N}-\text{N})$	1158	1147	1149	1151	1150
$\nu(\text{C}-\text{O})$	1066	1092	1090	1091	1085
$\nu_s(\text{C}-\text{O}-\text{C})_{\text{furan}}$	1017	1021	1035	1020	1019
$\omega(\text{OH})$	746	756	755	755	753
$\nu(\text{M}-\text{O})$	–	592	589, 532	565	588
$\nu(\text{M}-\text{N})$	–	475	484	488	445

*OH of the ligand

confirmed that it is free, no H-bond or metal binding, and the downfield shift of azomethine proton supported the participation of these groups in bonding to metal ion [42, 50]. The spectrum displayed the other bands at more or less the positions (Table 3).

Additionally, the ^{13}C -NMR spectrum of H_3L showed two signals at 165.0 and 159.5 ppm attributed to $\text{C}=\text{O}$ and phenyl-2 [42, 49], respectively. The signals at 149.7, 145.9 and 138.3 ppm were assigned to the furan-2, furan-5 and azomethine $\text{HC}=\text{N}$ [42, 49], respectively. The spectrum displayed several signals at 134.3, 128.9, 119.4, 117.7, 116.3, 114.6 and 112.7 ppm due to the phenyl-4, -6, -5, -3, furan-3, phenyl-1 and furan-4 [42, 49], respectively (Table 3). On contrary, the ^{13}C NMR spectrum of Zn(II) complex showed two signals at 173.4, 169.0 and 160.0 ppm attributed to azomethine ($\text{HC}=\text{N}$), enolized carbonyl ($\text{N}=\text{C}-\text{O}$) and phenyl-2 carbons [42, 49], respectively.

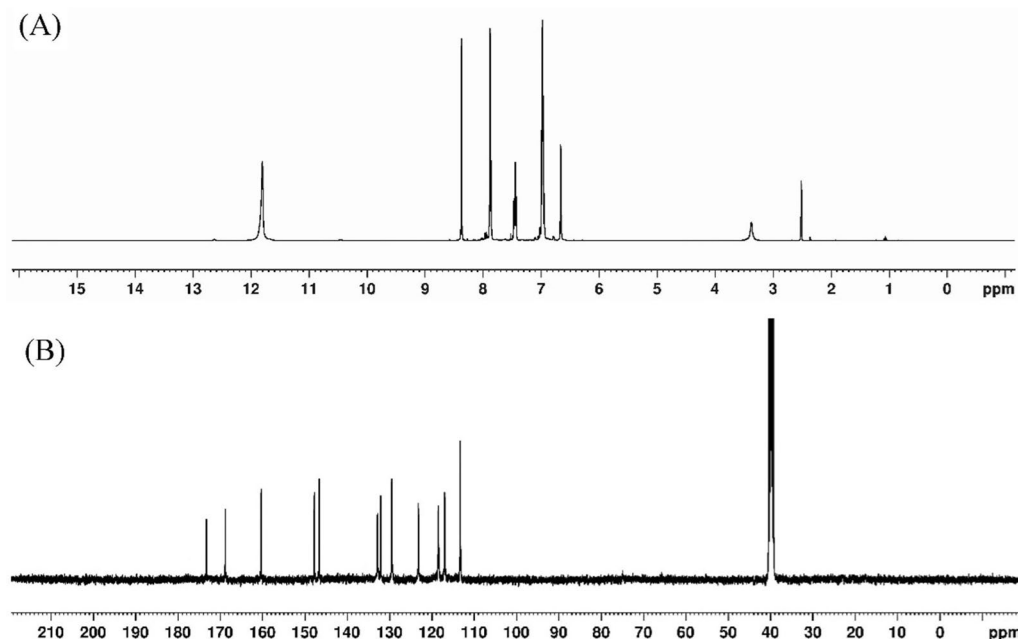


Fig. 2 A ^1H NMR of H_2L and B ^{13}C NMR spectrum of Zn(II) complex

Table 3 ^1H and ^{13}C -NMR data of H_2L and Zn(II) complex

Protons	$^1\text{H-NMR}$		$^{13}\text{C-NMR}$		
	H_2L	Zn(II)	Carbons	H_2L	Zn(II)
OH	11.80	13.98	C=O	165.0	169.0
NH	11.80	–	Ph-2	159.5	160.0
HC=N	8.37	8.59	Fur-2	149.7	147.9
Ph-6	7.86	7.74	Fur-5	145.9	146.7
Fur-5	7.86	7.52	C=N	138.3	173.4
Ph-4	7.44	7.34	Ph-4	134.3	132.9
Ph-3	6.97	6.89	Ph-6	128.9	132.0
Ph-5	6.97	6.89	Ph-5	119.4	123.2
Fur-3,4	6.65	6.66	Ph-3	117.7	118.6
			Fur-3	116.3	117.1
			Ph-1	114.6	129.6
			Fur-4	112.7	113.4

Mass spectra

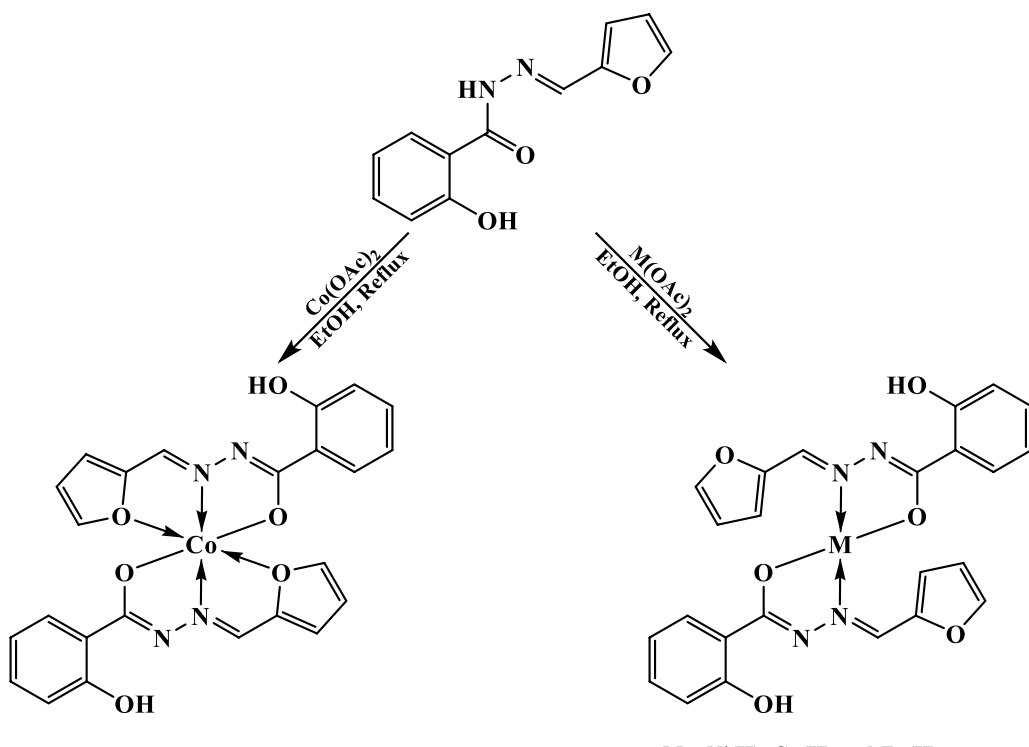
The mass spectrum of H_2L exhibits the molecular ion peak at $m/z=232.2$ corresponding to $[\text{M}+2]$ formula which in agreement with suggested ligand structure ($\text{C}_{12}\text{H}_{10}\text{N}_2\text{O}_3$; M.Wt. = 230.2) (Fig. 3A). Moreover, the spectrum displayed two peaks at $m/z=212.58$ (6.16%) and 197.07 (10.47%) which resulted from loss of OH and O fragments, respectively. The peak observed at $m/z=121.17$ (84.30%) was assigned to loss of phenyl ring to give $\text{C}_6\text{H}_5\text{N}_2\text{O}^\cdot$ (F. Wt. = 121.12) which underwent

two subsequent degradation steps by losing CN fragment in each, $m/z=67.37$ (9.86%), leading to formation of furan radical ($\text{C}_4\text{H}_3\text{O}^\cdot=67.02$). Finally, the base peak at $m/z=41.26$ (100.00%) was ascribed to the furan radical degradation by losing carbon monoxide moiety (CO) that led to formation of $\text{C}_3\text{H}_5^\cdot$ (F. Wt. = 41.07) (Scheme 2).

On the other hand, the mass spectra of the metal complexes presented good evidence of the suggested structure as they displayed molecular ion peak at $m/z=521.33$, 516.72 and 559.47 for Cu(II) (M. Wt. 521.98), Ni(II) (M. Wt. 517.12) and Zn(II) (M. Wt. 559.84) complexes, respectively (Additional file 1: Fig. S2). For instance, the Co(II) complex spectrum offered molecular ion peak at $m/z=519.19$ (28.20%) which corresponding to the $[\text{M}+2]$ formula (M. Wt. 517.36). Moreover, the spectrum displayed a base peak at $m/z=483.39$ (100.0%) which attributed to loss the two hydroxy groups giving $\text{C}_{24}\text{H}_{16}\text{CoN}_4\text{O}_4^{2-}$ (F. Wt. = 483.35) that afterward underwent loss of furan ring giving a peak at $m/z=416.48$ (36.63%) owing to the fragment $\text{C}_{20}\text{H}_{13}\text{CoN}_4\text{O}_3$ (F. Wt. = 416.28) (Fig. 3B). Further fragmentation steps were observed at $m/z=404.16$, 287.32 and 259.99 which resulted from losing carbon, benzaldehyde and nitrogen fragments, respectively (Scheme 3).

Electronic spectra and magnetic moments

The electronic spectrum of the H_2L ligand, in DMSO, displayed two bands, the first observed at $46,510\text{ cm}^{-1}$ attributed to the $\pi\rightarrow\pi^*$ transition of phenyl and furan

**Scheme 1** The suggested metal complexes structures

rings while the second were at $30,300\text{ cm}^{-1}$ and assigned to $\pi\rightarrow\pi^*$ transition of both carbonyl and azomethine groups [42]. In addition, a shoulder was observed at $21,740\text{ cm}^{-1}$ and ascribed to the $n\rightarrow\pi^*$ transition of the carbonyl and azomethine groups [42] (Fig. 4A).

On comparison with ligand spectrum, the Cu(II) complex's spectrum, in DMSO, displayed two bands at $46,510$ and $29,850\text{ cm}^{-1}$ with a shoulder at $25,316\text{ cm}^{-1}$ were assigned to the intra-ligand transitions ($\pi\rightarrow\pi^*$)_{Ar}, ($\pi\rightarrow\pi^*$)_{C=X} and ($n\rightarrow\pi^*$)_{C=X}, respectively (Fig. 4B). Furthermore, the two new bands at $23,256$ and $15,270\text{ cm}^{-1}$ were attributed to the ligand to metal charge transfer (LMCT) transition and $^2T\rightarrow^2E$ transition of tetrahedral geometry [51, 52] (Table 3). In addition, the complex exhibited magnetic moment 2.17 B.M. that is in the normal range of Cu(II) complexes regardless of their stereochemistry [52], $1.75\text{--}2.20\text{ B.M.}$.

In DMSO, the spectrum of the Co(II) complex was carried out and showed two bands at $16,395$ and $14,525\text{ cm}^{-1}$ attributed to $^4T_{1g}(F)\rightarrow^4T_{1g}(P)$ (v_3) and $^4T_{1g}(F)\rightarrow^4A_{2g}(P)$ (v_2) transitions, respectively, suggesting an octahedral geometry around the metal ion [51]. The band at $19,415\text{ cm}^{-1}$ was assigned to the ligand to metal charge transfer (LMCT) while the two bands observed at $25,315$ and $22,990\text{ cm}^{-1}$ were corresponding to the $n\rightarrow\pi^*$ transition of the azomethine groups (Additional file 1:

Fig. S3). The spectral data were utilized to estimate the ligand field parameters, v_1 , B and $10Dq$, using the spin allowed transitions of the d^7 -system and were found to be 6790 , 703 , and 7730 cm^{-1} , respectively, which were in the octahedral structure range [25, 51]. The magnetic moment of the Co(II) complex was found to be 5.16 B.M. , in accordance with the usual values of octahedral geometry, $4.3\text{--}5.2\text{ B.M.}$ [53] (Table 4).

Ni(II) complex spectrum presented a sharp band at $19,610\text{ cm}^{-1}$ in addition to a broad band at $15,505\text{ cm}^{-1}$ which assigned to LMCT and $^3T_1(F)\rightarrow^3T_1(P)$ (v_3) transitions, respectively, of tetrahedral geometry around Ni(II) ions [51]. Furthermore, the magnetic moment values of the complexes were found to be 3.39 B.M. , in accordance with the standard values of the tetrahedral geometry ($3.2\text{--}4.1\text{ B.M.}$) [51]. Finally, the Zn(II) complex displayed three bands at $46,510$, $29,850$ and $25,315\text{ cm}^{-1}$ along with two new bands at $23,256$ and $19,610\text{ cm}^{-1}$ attributed to intra-ligand transitions, ($\pi\rightarrow\pi^*$)_{Ar}, ($\pi\rightarrow\pi^*$)_{C=X}, ($n\rightarrow\pi^*$)_{C=X}, ($n\rightarrow\pi^*$)_{C=N*} [42] and LMCT [51, 52], respectively (Additional file 1: Fig. S3).

ESR spectra of Cu(II) complex

The ESR spectrum of Cu(II) complexes, that has tetragonal or distorted octahedral geometry, displayed g-tensor values $g_{||} > g_{\perp} > 2.0023$, which indicated that their ground

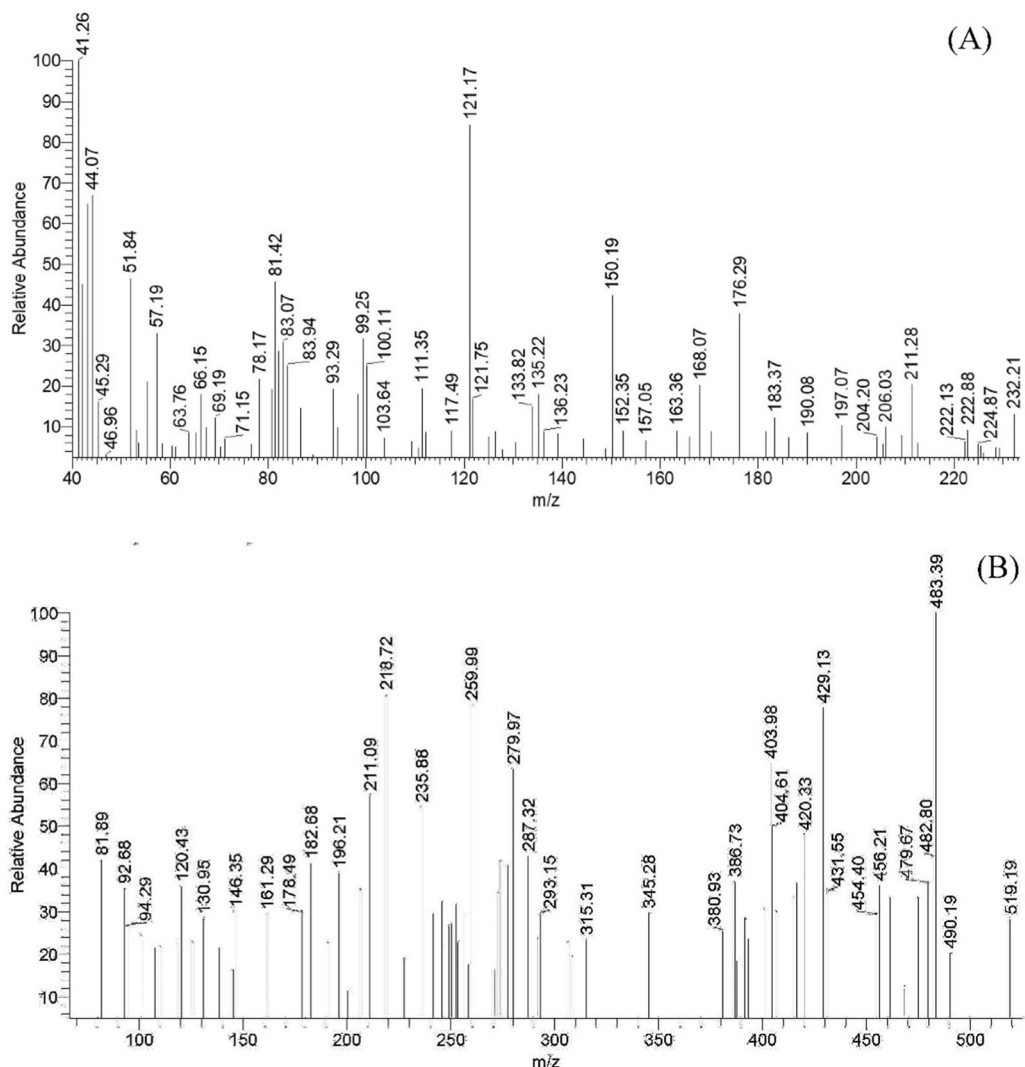
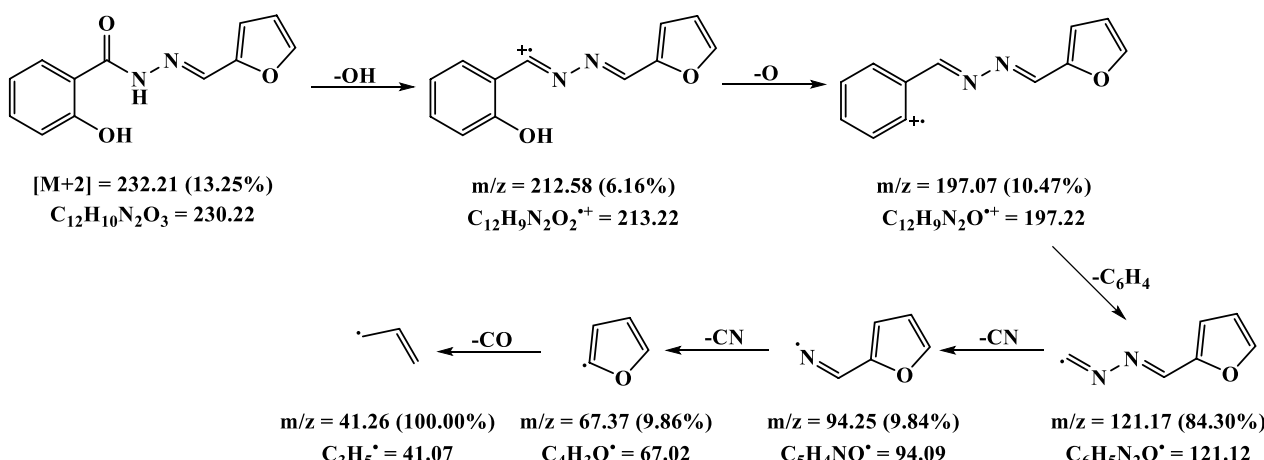
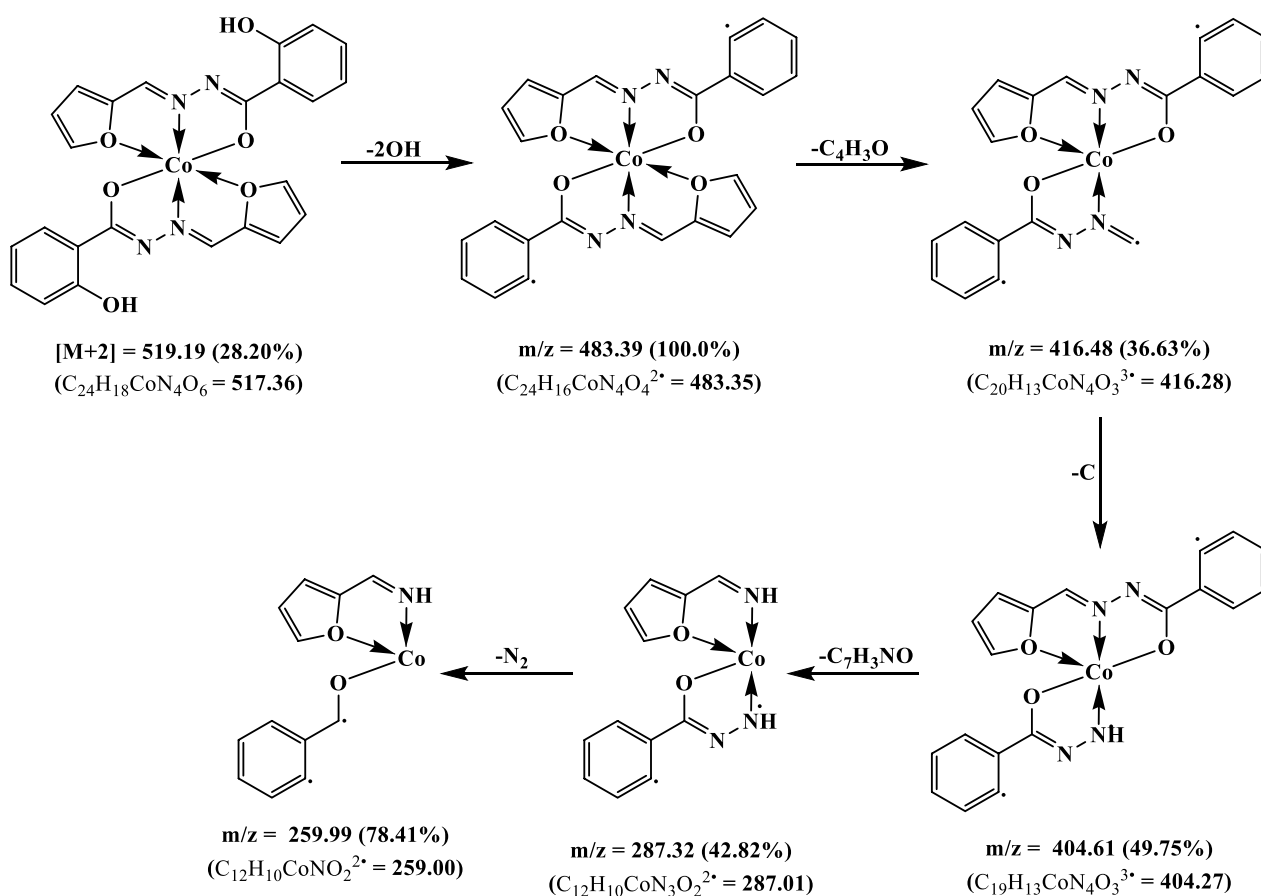


Fig. 3 The mass spectrum of the ligand (A) and Co(II) complex (B)



Scheme 2 The suggested fragmentation pattern of the ligand



Scheme 3 The suggested fragmentation pattern of Co^{2+} complex

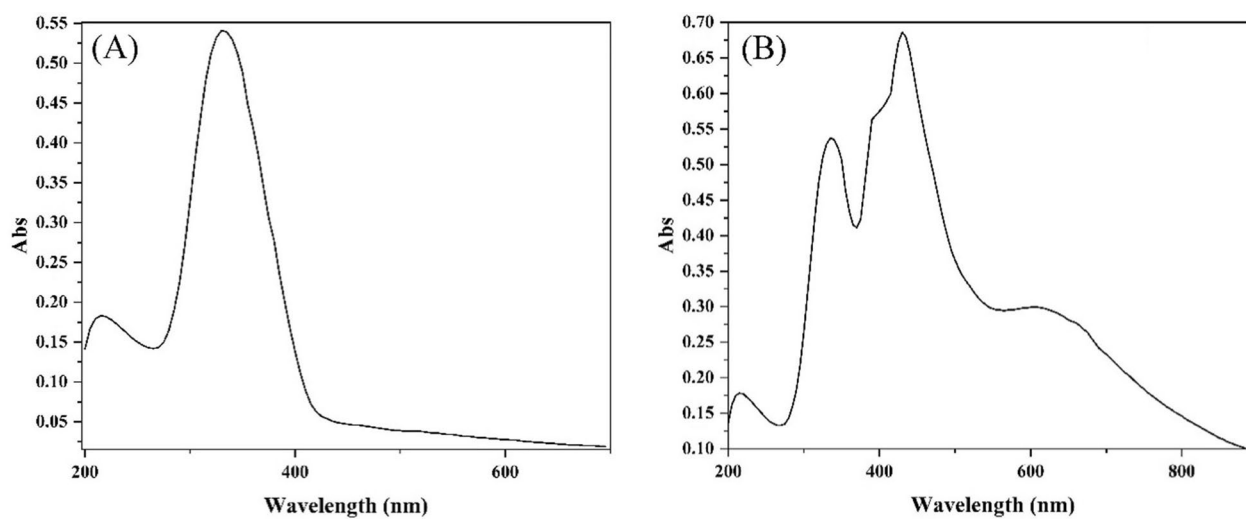
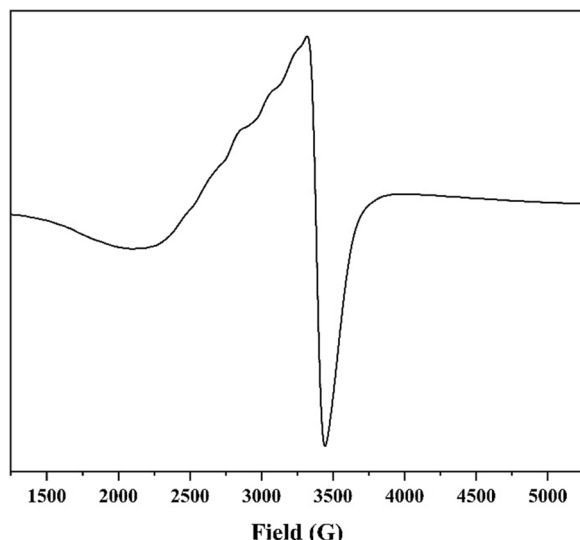


Fig. 4 The electronic spectrum of the ligand (A) and Cu^{2+} complex (B)

Table 4 Electronic spectra transitions and magnetic moment of H₂L and its complexes

Compound	Band position (cm ⁻¹) (transition)	μ_{eff} (B.M.)
H ₂ L	46,510 ($\pi \rightarrow \pi^*$) _{Ar} ; 30,300 ($\pi \rightarrow \pi^*$) _{C=X} ; 21,740 ($n \rightarrow \pi^*$) _{C=X}	–
Cu(II)	46,510 ($\pi \rightarrow \pi^*$) _{Ar} ; 29,850 ($\pi \rightarrow \pi^*$) _{C=X} ; 25,316 ($n \rightarrow \pi^*$) _{C=X} ; 23,256 (LMCT); 15,270 (${}^2T \rightarrow {}^2E$)	2.17
Co(II)	46,510 ($\pi \rightarrow \pi^*$) _{Ar} ; 29,850 ($\pi \rightarrow \pi^*$) _{C=X} ; 25,315 ($n \rightarrow \pi^*$) _{C=X} ; 22,990 ($n \rightarrow \pi^*$) _{C=N*} ; 19,415 (LMCT); 16,395 (${}^4T_{1g}(F) \rightarrow {}^4T_{1g}(P)(v_3)$); 14,525 (${}^4T_{1g}(F) \rightarrow {}^4A_{2g}(P)(v_2)$)	5.16
Ni(II)	46,510 ($\pi \rightarrow \pi^*$) _{Ar} ; 29,850 ($\pi \rightarrow \pi^*$) _{C=X} ; 25,315 ($n \rightarrow \pi^*$) _{C=X} ; 19,610 (LMCT); 15,505 (${}^3T_1(F) \rightarrow {}^3T_1(P)(v_3)$)	3.39
Zn(II)	46,510 ($\pi \rightarrow \pi^*$) _{Ar} ; 29,850 ($\pi \rightarrow \pi^*$) _{C=X} ; 25,315 ($n \rightarrow \pi^*$) _{C=X} ; 23,256 ($n \rightarrow \pi^*$) _{C=N*} ; 19,610 (LMCT)	–

**Fig. 5** The ESR spectrum of Cu(II) complex

state is [54]. In accordance, the solid-state spectrum of the Cu(II) complex presented g-tensor values of $g_{||} = 2.14$ and $g_{\perp} = 2.05$ which cleared out that the Cu(II) has a ground state with significant covalent nature of metal-ligand bonds as its $g_{||} < 2.3$ [55] (Fig. 5). If the value of the axial symmetry parameter G, who is defined as $(g_{||} - 2)/(g_{\perp} - 2)$, is less than 4, it indicates that the exchange interaction was reasonable and the local tetragonal axes were misaligned [56]. Consequently, the G value of the present Cu(II) complex was ascertained to be 3.10.

Furthermore, the decrease of $A_{||}$ with increasing $g_{||}$ is an evidence of increasing the tetrahedral distortion within the Cu(II) coordination sphere [52, 57]. To determine the distortion degree, the empirical index, $g_{||}/A_{||}$ factor, was calculated, where the square planar complexes revealed value in 105–135 range, while the distorted tetrahedral exhibited larger values [52, 58]. The spectrum displayed four hyperfine lines endorsing the monomeric nature of the Cu(II) complex ($A_{||} = 155 \times 10^{-4} \text{ cm}^{-1}$). Hence, the $g_{||}/A_{||}$ factor has been calculated to be 138, which implied the presence of significant dihedral angle

distortion in the xy-plane and tetrahedral distortion from square planar geometry [52].

As a measure of covalency, the orbital reduction factor, K, was determined using the following expressions (1–3) [59, 60], where K=1 for ionic, K<1 for covalent environments, $K_{||}$ and K_{\perp} are the parallel and perpendicular components of orbital reduction factor, respectively.

$$K_{||}^2 = \frac{(g_{||} - 2.0023)}{8 \times \lambda_o} \times \text{d-d transition} \quad (1)$$

$$K_{\perp}^2 = \frac{(g_{\perp} - 2.0023)}{2 \times \lambda_o} \times \text{d-d transition} \quad (2)$$

$$K^2 = \frac{(K_{||}^2 + 2K_{\perp}^2)}{3} \quad (3)$$

The results showed that the complex had K = 0.63, $K_{||} = 0.57$ and $K_{\perp} = 0.65$, indicating the strong ionic character and in-plane π -bonding as $K_{||} < K_{\perp}$.

Thermal analyses

To explore the isolated solid complexes thermal stability and aid in characterization of their chemical structures, thermal gravimetric analysis (TGA) of was carried out. The thermogram of the Cu(II) complex displayed the first degradation step at 165–335 °C region and was attributed to loss of hydroxy phenyl fragments ($C_{14}H_{10}O_2$) (Found 40.70; Calcd. 40.28%). The subsequent stage was observed at 335–475 °C and assigned to removal of furan rings along with other fragments, $C_{10}H_8NO_2$, (Found 33.70; Calcd. 33.37%). The third step has been extended from 475 to 1000 °C and ascribed to loss of nitrogen molecule (Found 4.97; Calcd. 5.37%) which led to a residue of $CuNO_2$ (Found 20.63; Calcd. 20.99%) (Fig. 6).

Likewise, the TG curve of the Co(II) complex exhibited three decomposition stages, the first stage at 180–330 °C

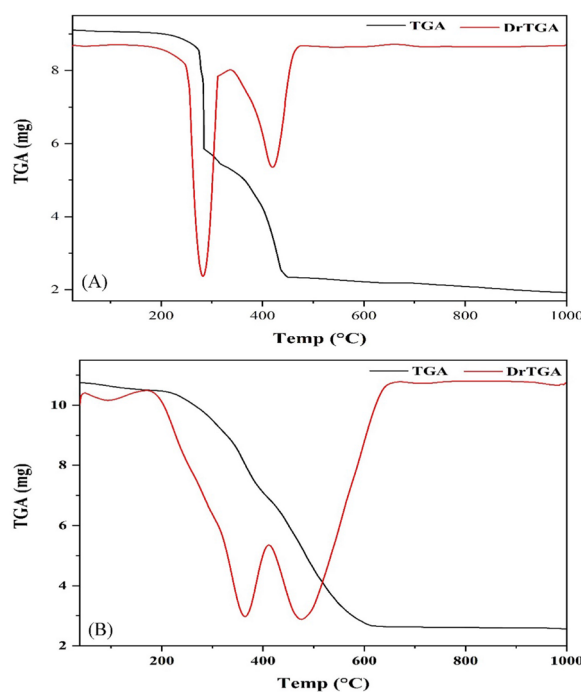


Fig. 6 The TG curves of Cu(II) (A) and Zn(II) (B) complexes

corresponding to loss of hydroxy phenyl in addition to hydroxyl moieties (Found 21.86; Calcd. 21.28%) whereas the second was observed in 330–482 °C range and assigned to degradation of the ligand through losing $C_{18}H_{12}NO_2$ (Found 52.90; Calcd. 53.03%) (Additional file 1: Fig. S4). Eventually, the 3rd stage was spread over the 482–1000 °C region and accompanied with losing of

nitrogen molecule to result in residue of $CoNO_2$ (Found 20.15; Calcd. 20.28%) (Table 5).

Alternatively, the Ni(II) complex graph showed only two broad degradation stages, the 1st was started at 185 to 375 °C and attributed to loss of hydroxy cyanophenyl fragments, $C_{14}H_{10}N_2O_2$, (Found 46.25; Calcd. 46.07%) (Additional file 1: Fig. S4). While, the 2nd was observed at 375–1000 °C and assigned to complete decomposition of the ligand resulting in a residue of NiO (Found 14.47; Calcd. 14.44%) (Table 5).

Finally, the TG curve of the Zn(II) complex presented the first degradation earlier than other complexes, 40–170 °C, where it was assigned to loss of the outside coordination sphere water molecule (Fig. 6). The second step was displayed at 170–413 °C region and attributed to loss of hydroxy phenyl fragments, $C_{12}H_{10}O_2$, (Found 34.03; Calcd. 34.37%) whereas the third one was observed at 413–1000 °C range due to decomposition of the ligand to give a residue of $Zn(CO)_2$ (Found 22.82; Calcd. 22.40%) (Table 5).

DFT computations

The DFT calculations were carried out to obtain the geometrically optimized structure in addition to the frontier molecular orbitals shapes and energy of the ligand and its metal complexes. The resulting geometrical parameters, bond length, angle and dihedral angle, were compared with those obtained from x-ray single crystal of analogous molecules [61, 62] where small difference was observed. The difference may be ascribed to that the theoretical calculations were carried out on single molecule in gaseous state, where no intermolecular columbic

Table 5 TGA of the isolated metal complexes

Complex	Temp. range (°C)	Wt. loss, %	Fragment	Fragment, %
Cu(II)	165–335	40.70	2HOPhC ($C_{14}H_{10}O_2$)	40.28
	335–475	33.70	2furanC+N ($C_{10}H_8NO_2$)	33.37
	475–1000	4.97	N_2	5.37
	Residue	20.63	$CoNO_2$	20.99
Co(II)	180–330	21.86	PhOH+OH ($C_6H_6O_2$)	21.28
	330–482	52.90	Lig. Dec. ($C_{18}H_{12}NO_2$)	53.03
	482–1000	5.09	N_2	5.41
	Residue	20.15	$CoNO_2$	20.28
Ni(II)	185–375	46.25	2HOPhCN ($C_{14}H_{10}N_2O_2$)	46.07
	375–1000	39.28	2furCN+O ($C_{10}H_8N_2O_3$)	39.49
	Residue	14.47	NiO	14.44
	40–170	3.31	H_2O	3.33
Zn(II)	170–413	34.03	2PhOH ($C_{12}H_{10}O_2$)	34.37
	413–1000	39.84	2FurCNN ($C_{10}H_8N_4O_2$)	39.90
	Residue	22.82	$Zn(CO)_2$	22.40

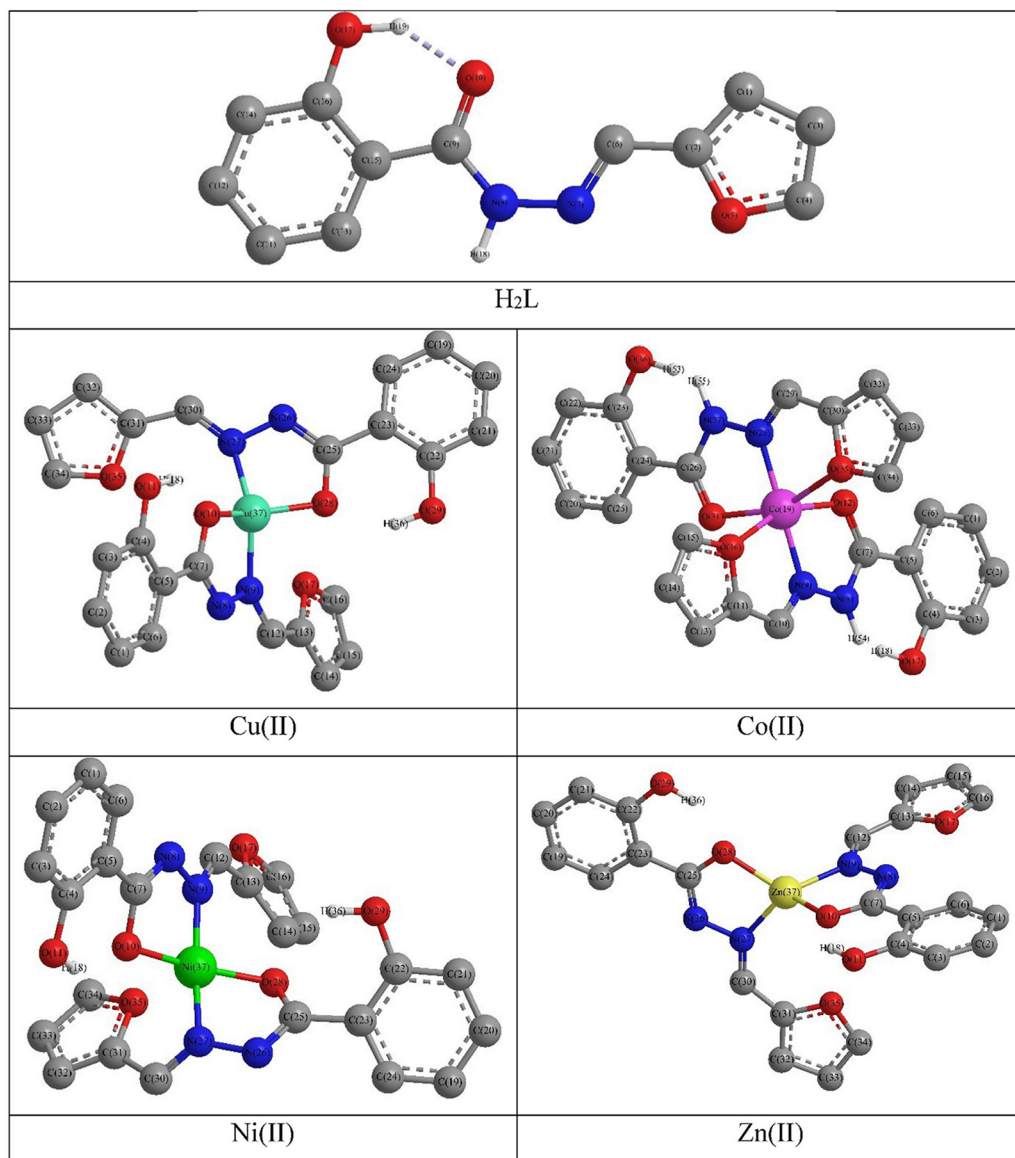


Fig. 7 The optimized structures of H_2L and its metal complexes

interactions, whereas, the experimental were acquired for molecules interacting in solid crystal lattice [63].

H_2L optimized structure disclosed that it has a planar structure in which the hydroxyl and carbonyl group were alongside but the hydroxyl's hydrogen atom was orient away from the carbonyl's oxygen, consequently, there are no H-bond (Additional file 1: Table S1). Meanwhile, the optimized structures of the metal complexes revealed that all have distorted tetrahedral except the Co(II) which has an octahedral stereochemistry in accordance with the suggested configurations (Fig. 7).

The comparison of geometrical parameters data of ligand with those of complexes reveal that:

- i) The ligand $\text{C}^2_{(\text{fur})}-\text{O}^1_{(\text{fur})}$ bond length was 1.40 Å and did not alter on coordination of the furfural oxygen to Co(II) ion (Additional file 1: Table S2).
- ii) In H_2L , the $\text{N}_{(\text{imin})}-\text{NH}_{(\text{Hz})}$ and $\text{CO}_{(\text{sal})}-\text{OC}_{(\text{sal})}$ bonds were 1.39 and 1.28 Å, while due their involvement of the $\text{N}_{(\text{imin})}$ and $\text{OC}_{(\text{sal})}$ in chelation to the metal ions and enolization, their lengths became in 1.27–1.40 and 1.22–1.35 Å range, respectively.
- iii) Generally, the metal complexes have distorted stereochemistries as indicated from the bond length data, i.e., $\text{M}-\text{N}_{(\text{imin})}$, 1.84–2.03 Å, was longer than $\text{M}-\text{OC}_{(\text{sal})}$, 1.80–1.95 Å.

iv) Moreover, the bond angles data presented another distortion in the geometrical configuration, e.g. in octahedral Co(II), the angles were deviate from the standard values, 90° and 180° by 2.0° to 11.0° (Additional file 1: Table S3).

Additionally, the highest occupied and lowest unoccupied molecular orbitals (HOMO and LUMO) govern how the molecule interact with other species where HOMO acts as electron donor while LUMO acts as electron acceptor [10, 33]. Thus, the higher the HOMO energy, the easier to donate electrons whereas LUMO accepts electrons easier when it has low energy [10, 33]. The LUMO-HOMO energy gap reflects the chemical activity of the molecule, where a molecule with a small energy gap is soft molecule, more polar, chemically reactive and less kinetically stable [64]. Also, the low HOMO-LUMO gap indicates facile charge transfer interaction taking place within the molecule [63].

The LUMO-HOMO plots for the ligand showed that the HOMO was mainly consisted of the non-bonding orbitals, that occupied by lone pair of electrons, of the oxygen and nitrogen atoms in addition to the π -orbitals of whole molecule while the LUMO was formed from the π^* -orbitals of the whole molecule. Thus, the HOMO-LUMO charge transfer may be described as $\pi \rightarrow \pi^*$ and $n \rightarrow \pi^*$ transitions. On the other hand, the octahedral metal complexes plot showed that their HOMO was mainly made of the π -orbital of the whole molecule and heteroatoms lone pair of electrons in addition to minor contribution of the metal ion. Whereas, their LUMO was constructed from the π^* -orbital of the molecule with contribution of the central metal ion. On contrary, the square planar Ni(II) complex has different FMO's configurations where the HOMO was built of the π -orbital of the phenyl ring and lone pair of electrons with minor involvement of the Ni(II) ion while the LUMO was made of the π^* -orbital of the furfural ring with more contribution of the metal (Fig. 8).

According the HOMO-LUMO energy data, the ligand has the highest HOMO energy, $E_H = -6.32$ eV, revealing its electron donation character while the metal complexes displayed close values, -5.71 to -6.06 eV. Moreover, the LUMO data indicated that the Ni(II) complex has the highest energy value, $E_L = -2.84$ eV. The calculated HOMO-LUMO energy gap, ΔE_{H-L} , of the ligand was the highest value, 4.05 eV, while, Ni(II) complex has the lowest, 3.07 eV (Table 6).

Finally, the E_H and E_L were used to estimate other chemical reactivity descriptors such as electronegativity (χ), which illustrate that molecule behaves has Lewis's acidic or basic character, and global hardness (η) which measure the charge transfer resistance [65]. Moreover,

the global softness (δ), describes the molecule receiving electrons capacity, and electrophilicity (ω) that measures of energy reduction due to HOMO-LUMO electron flow between, were calculated as follows, (4–9) [65]:

$$\chi = -\frac{1}{2}(E_{HOMO} + E_{LUMO}) \quad (4)$$

$$\eta = -\frac{1}{2}(E_{HOMO} - E_{LUMO}) \quad (5)$$

$$\delta = \frac{1}{\eta} \quad (6)$$

$$\omega = \frac{\chi^2}{8\eta} \quad (7)$$

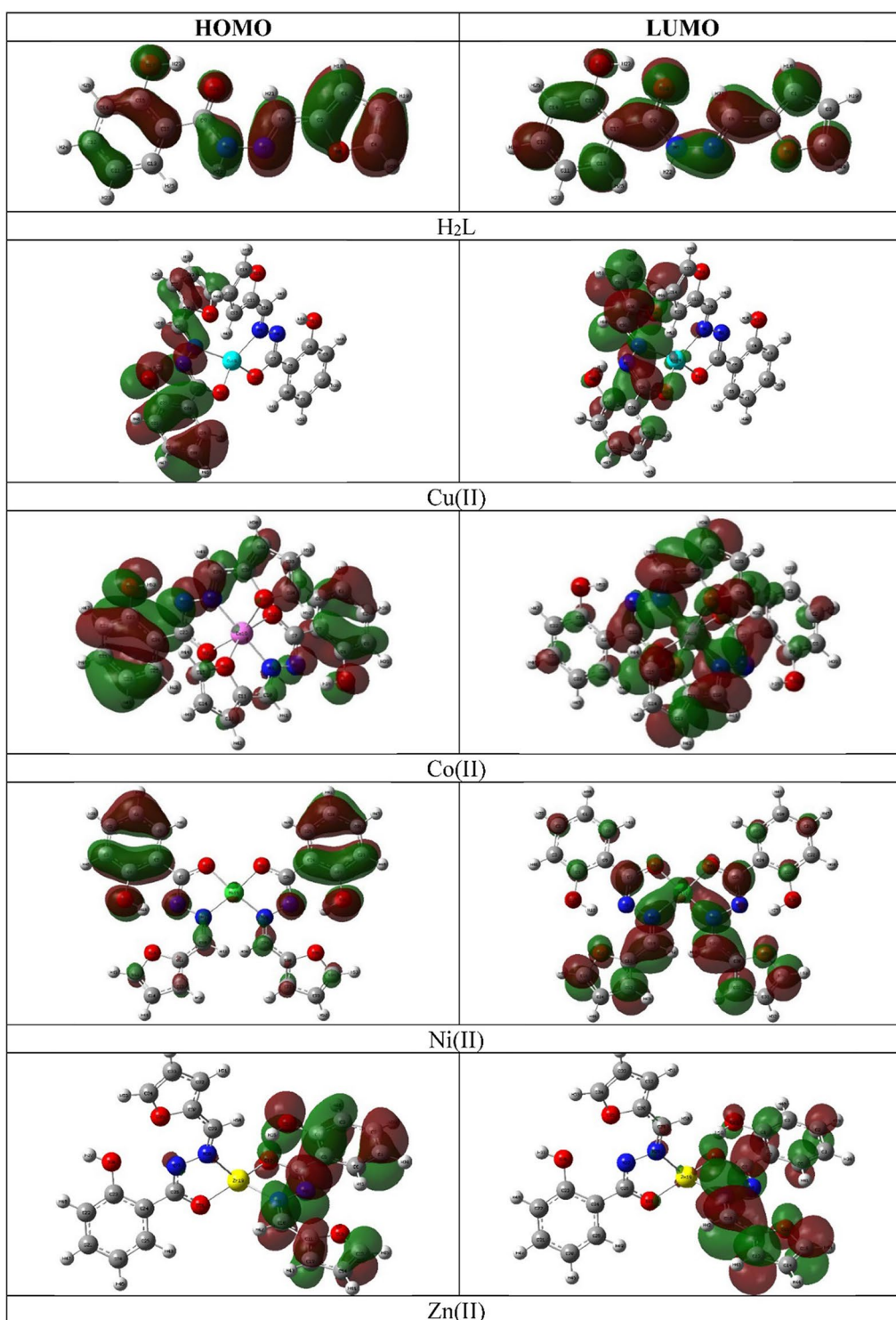
$$\omega^- = \frac{(3I + A)^2}{16(I - A)} \quad (8)$$

$$\omega^+ = \frac{(I + 3A)^2}{16(I - A)} \quad (9)$$

As shown in Table 6, the ligand displayed the highest global hardness, 2.02 eV, whereas the Ni(II) complex had the lowest value, 1.54 eV. On contrary, the softness presented reversed order where Ni(II) complex has the highest softness, 0.65 eV. The molecules with electrophilicity index (ω) > 1.5 eV, that measure of acquiring extra electronic charge from the environment stabilization energy, were considered as strong electrophile [66, 67]. Therefore, the studied compounds were strong electrophile as they exhibited ω index ranged from 4.56 to 6.23 eV following the order $L < Zn(II) < Co(II) < Cu(II) < Ni(II)$. Likewise, the electron donating (ω^+) and acceptance (ω^-) powers data, which demonstrated the capability to give and receive electrons, respectively, obeyed the previous order but they exhibited more donation tendency, 2.66–3.18 eV, than acceptance, 6.96–7.25 eV, where smaller values signify enhanced transaction [66, 67] (Table 6).

Cytotoxicity activity

The cytotoxicity of the ligand and its metal complexes has been evaluated in vitro against two cell lines, HePG-2 and HCT-116, which represent liver and colon cancer, respectively. Doxorubicin was used as a reference medication for comparison, and the results are shown in Table 7. The results revealed that the ligand exhibited moderate cytotoxicity towards HePG-2 and HCT-116 ($IC_{50} = 30.72$ and $35.40 \mu M$). Similarly, both of the Ni(II) and Zn(II) complexes exhibited moderate cytotoxicity

**Fig. 8** 3D plots of FMO's for H_2L and its complexes

($\text{IC}_{50} = 32.83\text{--}41.47 \mu\text{M}$). However, the Cu(II) and Co(II) complexes displayed weak impacts on the examined cell lines. It is noteworthy that the cytotoxicity of H_2L was

comparatively higher than that of metal complexes which may be correlated to the presence of several free active sites in H_2L which facilitate binding to the protein. But,

Table 6 The FMO's energies and chemical reactivity descriptors of the ligand and its complexes (eV)

Compound	E_H	E_L	ΔE_{H-L}	X	η	S	ω	$\omega+$	$\omega-$
H_2L	-6.32	-2.27	4.05	4.29	2.02	0.49	4.56	2.66	6.96
Cu(II)	-6.06	-2.83	3.23	4.45	1.61	0.62	6.13	4.11	8.55
Co(II)	-5.83	-2.58	3.25	4.21	1.62	0.62	5.45	3.55	7.76
Ni(II)	-5.91	-2.84	3.07	4.37	1.54	0.65	6.23	4.23	8.61
Zn(II)	-5.71	-2.41	3.29	4.06	1.65	0.61	5.01	3.18	7.25

Table 7 In vitro cytotoxic activity IC_{50} of the ligand and its complexes

Compound	In vitro cytotoxicity IC_{50} (μM)*	
	HePG-2	HCT-116
Doxorubicin	4.50 ± 0.2	5.23 ± 0.3
H_2L	30.72 ± 2.2	35.40 ± 2.2
Cu(II)	82.63 ± 4.2	> 100
Co(II)	93.56 ± 4.7	89.01 ± 4.5
Ni(II)	41.47 ± 2.6	39.19 ± 2.4
Zn(II)	32.83 ± 2.3	37.27 ± 2.4

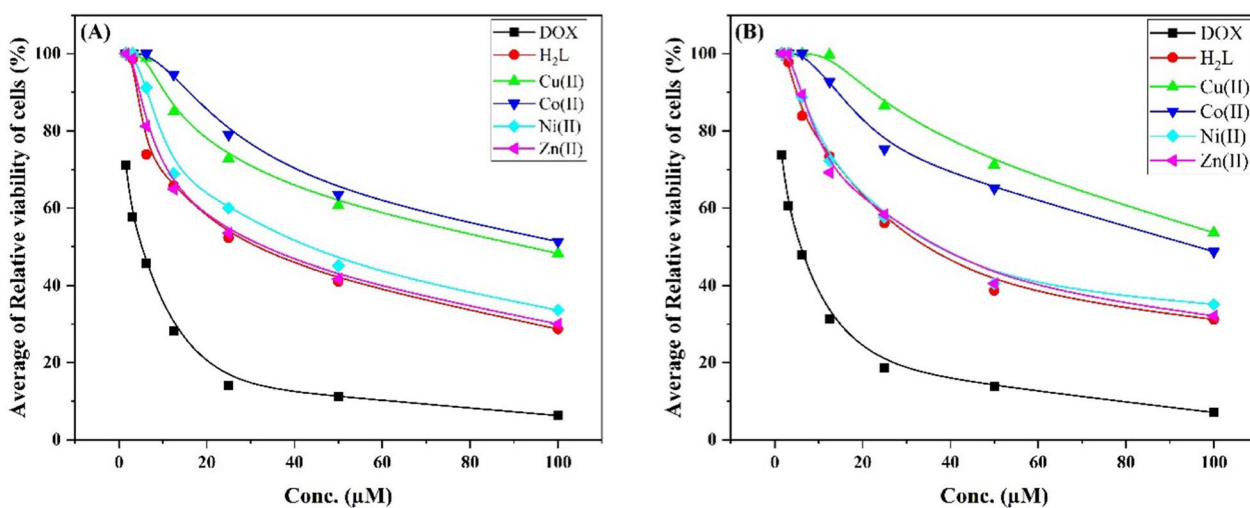
* IC_{50} (μM): 1–10 (very strong), 11–20 (strong), 21–50 (moderate), 51–100 (weak) and above 100 (non-cytotoxic)

after complexation, some of the active sites no longer available due to their involvement in metal ion chelation. Furthermore, the metal complexes have large size, since their stoichiometric ratio was 1:2 (M:L), which may hinder their ability to penetrate through the cell membrane and hence reduce the cytotoxic effects. Despite the value of IC_{50} , the Zn(II) complex was the most potent against the two cell lines. The average cells relative viability

percent for both cell lines presented that the ligand had the least viability and then the Zn(II) complex (Fig. 9).

Conclusion

The spectral analyses of *N'*-(furan-2-ylmethylene)-2-hydroxybenzohydrazideligand revealed its existence in the keto-form. While, upon reaction with the metal acetate, the resulting metal complexes have a 1:2 (M:L) stoichiometry and coordinated in enol-form as mononegative bidentate via enolic O and azomethine N, however, in Co(II) complex, the ligand was reacted in mononegative tridentate manner through enolic and furan O in addition to azomethine N. The energy gap of FMO's, determined by DFT computations, showed that the ligand and Ni(II) complex have the highest and lowest values, respectively, following the order $H_2L > Zn(II) > Co(II) > Cu(II) > Ni(II)$. The cytotoxicity activity against two cell lines, HePG-2 and HCT-116, of H_2L was relatively higher (lower IC_{50}) than that of metal complexes, $H_2L < Zn(II) < Ni(II) < Cu(II) < Co(II)$ which may be correlated to blocking of some active sites in H_2L that bonded to the metal ions.

**Fig. 9** The cell viability (%) of the ligand and its complexes against HePG-2 (A) and HCT-116 (B)

Supplementary Information

The online version contains supplementary material available at <https://doi.org/10.1186/s13065-023-01098-8>.

Additional file 1: Figure S1. IR spectra of Cu(II), Ni(II) and Zn(II) complexes. **Figure S2.** The mass spectra of Cu(II) (A), Ni(II) (B) and Zn(II) (C) complexes. **Figure S3.** The electronic spectra of Co(II) (A), Ni(II) (B) and Zn(II) (C) complexes. **Figure S4.** The TG curves of Co(II) (A) and Ni(II) (B) complexes. **Table S1.** Bond length data of the ligand and its complexes. **Table S2.** Bond angle data of the ligand and its complexes. Table S3. Dihedral angle data of the ligand and its complexes.

Author contributions

All authors contributed to the study conception and design. Material preparation, data collection and analysis were performed by NMH, GS, and MHA. The first draft of the manuscript was written by NMH and all authors commented on previous versions of the manuscript. All authors read and approved the final manuscript.

Funding

Open access funding provided by The Science, Technology & Innovation Funding Authority (STDF) in cooperation with The Egyptian Knowledge Bank (EKB).

Availability of data and materials

The datasets used and/or analyzed during the current study are available from the corresponding author on reasonable request.

Declarations

Ethics approval and consent to participate

Not applicable.

Consent for publication

Not applicable.

Competing interests

The authors declare that they have no known competing financial interests or personal relationships that could have appeared to influence the work reported in this paper.

Author details

¹Chemistry Department, Faculty of Science, Port Said University, P.O. Box 4252, Port-Said, Egypt. ²Chemistry Department, Faculty of Science, Mansoura University, Mansoura, Egypt.

Received: 26 July 2023 Accepted: 30 November 2023

Published online: 28 January 2024

References

- Uddin MN, Ahmed SS, Alam SMR. Biomedical applications of Schiff base metal complexes. *J Coord Chem.* 2020;73:3109–49.
- Ikram M, Rehman S, Khan A, Baker RJ, Hofer TS, Subhan F, Qayum M, Schulzke C. Synthesis, characterization, antioxidant and selective xanthine oxidase inhibitory studies of transition metal complexes of novel amino acid bearing Schiff base ligand. *Inorg Chim Acta.* 2015;428:117–26.
- Abdel-Rahman LH, El-Khatib RM, Nassr LA, Abu-Dief AM, Lashin FE-D. Design, characterization, teratogenicity testing, antibacterial, antifungal and DNA interaction of few high spin Fe(II) Schiff base amino acid complexes. *Spectrochim Acta A Mol Biomol Spectrosc.* 2013;111:266–76.
- Mohamad ADM, Abualreish M, Abu-Dief AM. Antimicrobial and anticancer activities of cobalt (III)-hydrazone complexes: solubilities and chemical potentials of transfer in different organic co-solvent–water mixtures. *J Mol Liq.* 2019;290:111162.
- Mukherjee S, Chowdhury S, Chattapadhyay AP, Bhattacharya A. Spectroscopic, cytotoxic and DFT studies of a luminescent palladium (II) complex of a hydrazone ligand that induces apoptosis in human prostate cancer cells. *Inorg Chim Acta.* 2011;373:40–6.
- Fouda AE-AS, Abd El-Maksoud SA, El-Sayed EH, Elbaz HA, Abousalem AS. Effectiveness of some novel heterocyclic compounds as corrosion inhibitors for carbon steel in 1 M HCl using practical and theoretical methods. *RSC Adv.* 2021;11:19294–309.
- Sherif YE, Hosny NM. Synthesis, characterization, and anti-rheumatic potential of phthalazine-1, 4-dione and its Cu (II) and Zn (II) complexes. *Med Chem Res.* 2014;23:2536–42.
- Hosny NM, Sherif YE. Synthesis, structural, optical and anti-rheumatic activity of metal complexes derived from (E)-2-amino-N-(1-(2-aminophenyl) ethylidene) benzohydrazide (2-AAB) with Ru(III), Pd(II) and Zr(IV). *Spectrochim Acta A Mol Biomol Spectrosc.* 2015;136:510–9.
- Jungreis E, Thabet S. Analytical applications of Schiff bases. *Chelates Anal Chem.* 1969;2:149–77.
- Latif MA, Ahmed T, Hossain MS, Chaki BM, Abdou A, Kudrat-E-Zahan M. Synthesis, spectroscopic characterization, DFT calculations, antibacterial activity, and molecular docking analysis of Ni (II), Zn (II), Sb (III), and U (VI) metal complexes derived from a nitrogen-sulfur Schiff base. *Russ J Gen Chem.* 2023;93:389–97.
- Chaturvedi D, Kamboj M. Role of Schiff base in drug discovery research. *Chem Sci J.* 2016;7:7–8.
- Sumrra SH, Zafar W, Javed H, Zafar M, Hussain MZ, Imran M, Nadeem MA. Facile synthesis, spectroscopic evaluation and antimicrobial screening of metal endowed triazole compounds. *Biometals.* 2021;34:1329–51.
- Sumrra SH, Zafar W, Malik SA, Mahmood K, Shafqat SS, Arif S. Metal based bioactive nitrogen and oxygen donor mono and bis Schiff bases: design, synthesis, spectral characterization, computational analysis and antibacterial screening. *Acta Chim Slov.* 2022. <https://doi.org/10.17344/acsi.2021.7182>.
- Rani S, Sumrra SH, Chohan ZH. Metal based sulfonilamides: a note on their synthesis, spectral characterization, and antimicrobial activity. *Russ J Gen Chem.* 2017;87:1834–42.
- Jadhav B, Yamgar R, Mali SN. Synthesis and anti-tuberculosis activity of substituted 3, 4-(dicoumarin-3-yl)-2, 5-diphenyl furans and pyrroles. *Eng Proc.* 2022;31:78.
- El-Obeid HA, Elnima El, Al-Badr AA. Synthesis and antimicrobial activity of new furan derivatives. *Pharm Res.* 1985;2:42–3.
- Wu X, Pang X-J, Xu L-L, Zhao T, Long X-Y, Zhang Q-Y, Qin H-L, Yang D-F, Yang X-L. Two new alkylated furan derivatives with antifungal and anti-bacterial activities from the plant endophytic fungus *Emericella* sp. XI029. *Nat Prod Res.* 2018;32:2625–31.
- Eldehna WM, Nocentini A, Elsayed ZM, Al-Warhi T, Aljaeed N, Alotaibi OJ, Al-Sanea MM, Abdel-Aziz HA, Supuran CT. Benzofuran-based carboxylic acids as carbonic anhydrase inhibitors and antiproliferative agents against breast cancer. *ACS Med Chem Lett.* 2020;11:1022–7.
- Samy F, Shebl M. Co (II), Ni (II), and Cu (II) complexes of 4, 6-bis (2-hydroxynaphthalen-1-yl) methyl-ene) hydrazono) ethyl) benzene-1, 3-diol: synthesis, spectroscopic, biological, and theoretical studies. *Appl Organomet Chem.* 2022;36: e6650.
- Abdel Halim S, Shebl M. Synthesis, spectral, structural, dft and nlo studies of cerium (III) and thorium (IV) complexes of 1-(5-(1-(2-aminophenylimino)ethyl)-2, 4-dihydroxyphenyl) ethanone. *J Coord Chem.* 2022;74:2984–3001.
- Hosny NM, El Morsy ESA, Sherif YE. Synthesis, spectral, optical and anti-inflammatory activity of complexes derived from 2-aminobenzohydrazide with some rare earths. *J Rare Earths.* 2015;33:758–64.
- Abdel-Rhman MH, Motawea R, Belal A, Hosny NM. Spectral, structural and cytotoxicity studies on the newly synthesized n'1, n'3-diisonicotinoylmalonohydrazide and some of its bivalent metal complexes. *J Mol Struct.* 2022;1251:131960.
- Noorussabah N, Choudhary M, Das N, Mohan B, Singh K, Singh RK, Ahmad K, Muhammad S, Kumar S. Copper (II) and nickel (II) complexes of tridentate hydrazide and Schiff base ligands containing phenyl and naphthalyl groups: synthesis, structural, molecular docking and density functional study. *J Inorg Organomet Polym Mater.* 2020;30:4426–40.

24. Khalid S, Sumra SH, Chohan ZH. Isatin endowed metal chelates as anti-bacterial and antifungal agents. *Sains Malays.* 2020;49:1891–904.
25. Orif MI, Abdel-Rhman MH. Synthesis, spectral and structural studies on some new isonicotinic thiosemicarbazide complexes and its biological activity. *Polyhedron.* 2015;98:162–79.
26. Hosny NM, Hassan NY, Mahmoud HM, Abdel-Rhman MH. Spectral, optical and cytotoxicity studies on 2-isonicotinoyl-N-phenylhydrazine-1-carboxamide (H_3L) and some of its metal complexes. *J Mol Struct.* 2018;1156:602–11.
27. Orie MI, Abdel-Rhman MH. Molecular modeling, spectroscopic and structural studies on newly synthesized ligand *N*-benzoyl-2-isonicotinoylhydrazine-1-carboxamide. *J Mol Struct.* 2018;1173:332–40.
28. Abdel-Rhman MH, Hussian MA, Mahmoud HM, Hosny NM. Synthesis, characterization, molecular docking and cytotoxicity studies on *N*-benzyl-2-isonicotinoylhydrazine-1-carbothioamide and its metal complexes. *J Mol Struct.* 2019;1196:417–28.
29. Hosny NM, Mahmoud HM, Abdel-Rhman MH. Spectral, optical, and cytotoxicity studies on *N*-(2-isonicotinoylhydrazine-carbonothioyl) benzamide and its metal complexes. *Heteroat Chem.* 2018;29:e21415.
30. Hosny NM, Hassan NY, Mahmoud HM, Abdel-Rhman MH. Synthesis, characterization and cytotoxicity of new 2-isonicotinoyl-N-phenylhydrazine-1-carbothioamide and its metal complexes. *Appl Organomet Chem.* 2019;33:e4998.
31. Hosny NM, Sheriff Y. Molecular docking study on some isonicotinoyl hydrazide derivatives as potential inhibitors of covid-19. *Lett Appl NanoBio-Science.* 2020;3:1217–24.
32. Jeffery G, Bassett J, Mendum J, Denney R. Vogel's quantitative chemical analysis. 5th ed. Essex: Longman Scientific and Technical Longman Group UK Limited; 1989.
33. Abdel-Rhman MH, El-Asmy AA, Ibrahim R, Hosny NM. New Schiff base ligand and some of its coordination compounds: synthesis, spectral, molecular modeling and biological studies. *J Mol Struct.* 2023;1279: 135023.
34. Frisch M, Trucks G, Schlegel H, Scuseria G, Robb M, Cheeseman J, Scalmani G, Barone V, Mennucci B, Petersson G. Gaussian. Inc., Wallingford, CT, USA; 2009.
35. Becke AD. Density functional thermochemistry. III. The role of exact exchange. *J Chem Phys.* 1993;98:5648–52.
36. Lee C, Yang W, Parr RG. Development of the Colle–Salvetti correlation-energy formula into a functional of the electron density. *Phys Rev B Condens Matter.* 1988;37:785–9.
37. Perdew JP, Wang Y. Pair-distribution function and its coupling-constant average for the spin-polarized electron gas. *Phys Rev B Condens Matter.* 1992;46:12947–54.
38. Dennington R, Keith T, Millam J. Semichem Inc., Shawnee Mission, KS; 2009.
39. Mosmann T. Rapid colorimetric assay for cellular growth and survival: application to proliferation and cytotoxicity assays. *J Immunol Methods.* 1983;65:55–63.
40. Denizot F, Lang R. Rapid colorimetric assay for cell growth and survival: modifications to the tetrazolium dye procedure giving improved sensitivity and reliability. *J Immunol Methods.* 1986;89:271–7.
41. Geary WJ. The use of conductivity measurements in organic solvents for the characterisation of coordination compounds. *Coord Chem Rev.* 1971;7:81–122.
42. Silverstein R, Webster F, Kiemle D. Spectrometric identification of organic compounds. 7th ed. Hoboken: Wiley; 2006.
43. Hosny NM, Mahmoud MAM, Aly MRE. 2-Hydroxybenzaldehyde-(4,6-dimethylquinolin-2-yl)-hydrazone (HBDH), synthesis, characterization, and ligational behavior towards some metals. *Synth React Inorg Metal-Org Nano-Metal Chem.* 2010;40:439–46.
44. Cross AHJ, Stevens SGE, Watts THE. Some characteristic infra-red absorption frequencies of furan compounds. I. *J Appl Chem.* 1957;7:562–5.
45. Al-Mohameed AM, AlFarraj ES, Al Onazi WA, Alothman AA, Almarhoon ZM. Synthesis, characterization, density functional theory, thermal, antimicrobial efficacy, and DNA binding/cleavage studies of Cu (II), Cr (III), Fe (III), Ni (II), Co (II), Zn (II), and Pt (IV) complexes with a derivative of 2-hydroxyphenoxymethylfuran-5-carbaldehyde. *J Chin Chem Soc.* 2020;67:2100–17.
46. Ferraro JR. Low-frequency vibrations of inorganic and coordination compounds. New York: Springer Science and Business Media; 2012.
47. Hosny NM, Hussian MA, Motawa R, Belal A, Abdel-Rhman MH. Synthesis, spectral, modeling, docking and cytotoxicity studies on 2-(2-aminobenzoyl)-N-ethylhydrazine-1-carbothioamide and its divalent metal complexes. *Appl Organomet Chem.* 2020;34:e5922.
48. Hosny NM, Belal A, Motawa R, Hussian MA, Abdel-Rhman MH. Spectral characterization, DFT, docking and cytotoxicity of *N*-benzyl-4, 5-dihydro-3-methyl-5-oxo-1H-pyrazole-4-carbothioamide and its metal complexes. *J Mol Struct.* 2021;1232:130020.
49. Rahim F, Ullah H, Taha M, Wadood A, Javed MT, Rehman W, Nawaz M, Ashraf M, Ali M, Sajid M. Synthesis and in vitro acetylcholinesterase and butyryl-cholinesterase inhibitory potential of hydrazide based Schiff bases. *Bioorg Chem.* 2016;68:30–40.
50. El-Gammal OA, Abdel-Latif E, Farag MG, Abdel-Rhman MH. Synthesis, characterization, and anticancer activity of new binuclear complexes of 2,2'-malonylbis(*N*-phenylhydrazine-1-carbothioamide). *Appl Organomet Chem.* 2021;35:e6194.
51. Lever ABP. Inorganic electronic spectroscopy. 1st ed. Amsterdam: Elsevier Publishing Company; 1968.
52. Hassanien MM, Gabr IM, Abdel-Rhman MH, El-Asmy AA. Synthesis and structural investigation of mono-and polynuclear copper complexes of 4-ethyl-1-(pyridin-2-yl) thiosemicarbazide. *Spectrochim Acta A Mol Biomol Spectrosc.* 2008;71:73–9.
53. Geeta B, Shrivankumar K, Reddy PM, Ravikrishna E, Sarangapani M, Reddy KK, Ravinder B. Binuclear cobalt (II), nickel (II), copper (II) and palladium (II) complexes of a new Schiff-base as ligand: synthesis, structural characterization, and antibacterial activity. *Spectrochim Acta A Mol Biomol Spectrosc.* 2010;77:911–5.
54. Hathaway BJ. A new look at the stereochemistry and electronic properties of complexes of the copper (II) ion. In complex chemistry. *Struct Bond.* 1984;57:55–118.
55. Kivelson D, Neiman R. ESR studies on the bonding in copper complexes. *J Chem Phys.* 1961;35:149–55.
56. Speier G, Csihony J, Whalen AM, Pierpont CG. Studies on aerobic reactions of ammonia/3, 5-di-tert-butylcatechol Schiff-base condensation products with copper, copper (I), and copper (II). Strong copper (II)-radical ferromagnetic exchange and observations on a unique N–N coupling reaction. *Inorg Chem.* 1996;35:3519–24.
57. Kasumov VT, Köksal F, Köseoglu R. Synthesis, spectroscopy and redox chemistry of bis(*n*-aryl-3,5-di-tert-butylsalicylaldiminato)copper(II) complexes. *J Coord Chem.* 2004;57:591–603.
58. Yokoi H, Addison A. Spectroscopic and redox properties of pseudotetrahedral copper (II) complexes. Their relation to copper proteins. *Inorg Chem.* 1977;16:1341–9.
59. Hathaway B. Structure and bonding, vol. 14. Berlin: Springer Verlag; 1973. p. 60.
60. Hosny NM, Ibrahim OA, Belal A, Hussian MA, Abdel-Rhman MH. Synthesis, characterization, DFT, cytotoxicity evaluation and molecular docking of a new carbothioamide ligand and its coordination compounds. *Res Chem.* 2023;5: 100776.
61. Hernández W, Carrasco F, Vaisberg A, Spodine E, Icker M, Krautscheid H, Beyer L, Tamariz-Angeles C, Olivera-Gonzales P. Novel thiosemicarbazone derivatives from furan-2-carbaldehyde: synthesis, characterization, crystal structures, and antibacterial, antifungal, antioxidant, and antitumor activities. *J Chem.* 2023. <https://doi.org/10.1155/2023/5413236>.
62. Hernández W, Paz J, Carrasco F, Vaisberg A, Manzur J, Spodine E, Hennig L, Sieler J, Beyer L. Synthesis and characterization of new palladium (II) complexes with ligands derived from furan-2-carbaldehyde and benzaldehyde thiosemicarbazone and their in vitro cytotoxic activities against various human tumor cell lines. *Z für Naturforschung B.* 2010;65:1271–8.
63. Sajan D, Joseph L, Vijayan N, Karabacak M. Natural bond orbital analysis, electronic structure, non-linear properties and vibrational spectral analysis of l-histidinium bromide monohydrate: a density functional theory. *Spectrochim Acta A Mol Biomol Spectrosc.* 2011;81:85–98.
64. Suresh D, Amalanathan M, Sebastian S, Sajan D, Joe IH, Jothy VB, Nemec I. Vibrational spectral investigation and natural bond orbital analysis of pharmaceutical compound 7-amino-2, 4-dimethylquinolinium formate-DFT approach. *Spectrochim Acta A Mol Biomol Spectrosc.* 2013;115:595–602.
65. Xavier S, Periandy S, Ramalingam S. NBO, conformational, NLO, HOMO–LUMO, NMR and electronic spectral study on 1-phenyl-1-propanol by quantum computational methods. *Spectrochim Acta A Mol Biomol Spectrosc.* 2015;137:306–20.

66. Afolabi SO, Semire B, Akiode OK, Idowu MA. Quantum study on the opto-electronic properties and chemical reactivity of phenoxazine-based organic photosensitizer for solar cell purposes. *Theor Chem Acc.* 2022;141:1–14.
67. Domingo LR, Rios-Gutierrez M, Perez P. Applications of the conceptual density functional theory indices to organic chemistry reactivity. *Molecules.* 2016;21: 748.

Publisher's Note

Springer Nature remains neutral with regard to jurisdictional claims in published maps and institutional affiliations.

Ready to submit your research? Choose BMC and benefit from:

- fast, convenient online submission
- thorough peer review by experienced researchers in your field
- rapid publication on acceptance
- support for research data, including large and complex data types
- gold Open Access which fosters wider collaboration and increased citations
- maximum visibility for your research: over 100M website views per year

At BMC, research is always in progress.

Learn more biomedcentral.com/submissions

